LETTERS
PUBLISHED ONLINE: 16 DECEMBER 2012 | DOI: 10.1038/NMAT3510

nature materials

A scalable neuristor built with Mott memristors

Matthew D. Pickett*, Gilberto Medeiros-Ribeiro and R. Stanley Williams

The Hodgkin–Huxley model for action potential generation in biological axons[1] is central for understanding the computational capability of the nervous system and emulating its functionality. Owing to the historical success of silicon complementary metal-oxide-semiconductors, spike-based computing is primarily confined to software simulations[2-4] and specialized analogue metal-oxide-semiconductor field-effect transistor circuits[5-8]. However, there is interest in constructing physical systems that emulate biological functionality more directly, with the goal of improving efficiency and scale. The neuristor[9] was proposed as an electronic device with properties similar to the Hodgkin–Huxley axon, but previous implementations were not scalable[10-13]. Here we demonstrate a neuristor built using two nanoscale Mott memristors, dynamical devices that exhibit transient memory and negative differential resistance arising from an insulating-to-conducting phase transition driven by Joule heating. This neuristor exhibits the important neural functions of all-or-nothing spiking with signal gain and diverse periodic spiking, using materials and structures that are amenable to extremely high-density integration with or without silicon transistors.

Signal transduction in neurons is mediated in large part by sodium and potassium ion channels that dynamically permit or prevent polarizing currents to charge or discharge through the cell membrane. If a cell body is sufficiently polarized through its dendritic inputs, the ion channels change conductance markedly and a voltage spike, or action potential, is triggered that travels along the axon. This all-or-nothing spiking has long been thought to be the fundamental process of computation in biology[14]. Although the detailed biochemistry of neurons is much more complicated than this simple picture, artificial neuron circuits have historically focused on approximating this spiking behaviour by mimicking the Hodgkin–Huxley model[1], which mathematically abstracts these two switching channels as coupled differential equations that define four state variables. From a circuit theoretic standpoint, the Na and K ion channels of the Hodgkin–Huxley model are mathematically equivalent to two distinct memristors[15] and their ability to generate action potentials is related to two important properties: local activity and edge of chaos[16,17].

Mott insulators[18] such as NbO_2 have long been known to exhibit current-controlled negative differential resistance[19,20], frequently referred to as threshold switching, when used in two-terminal devices. This phenomenon is caused by a reversible insulator-to-metal phase transition[18,21,22], which occurs when sufficient current is driven through the device to locally heat some of the material above its transition temperature, thus inducing a conductive channel in the device that bridges the two electrodes. As injecting sufficient energy into these devices to heat the material to its conducting state requires a measurable time, they are dynamical systems with a resistance that is dependent on excitation history. Given this hysteretic property and the purely dissipative nature of these devices, the canonical memristor formalism[15] is the correct

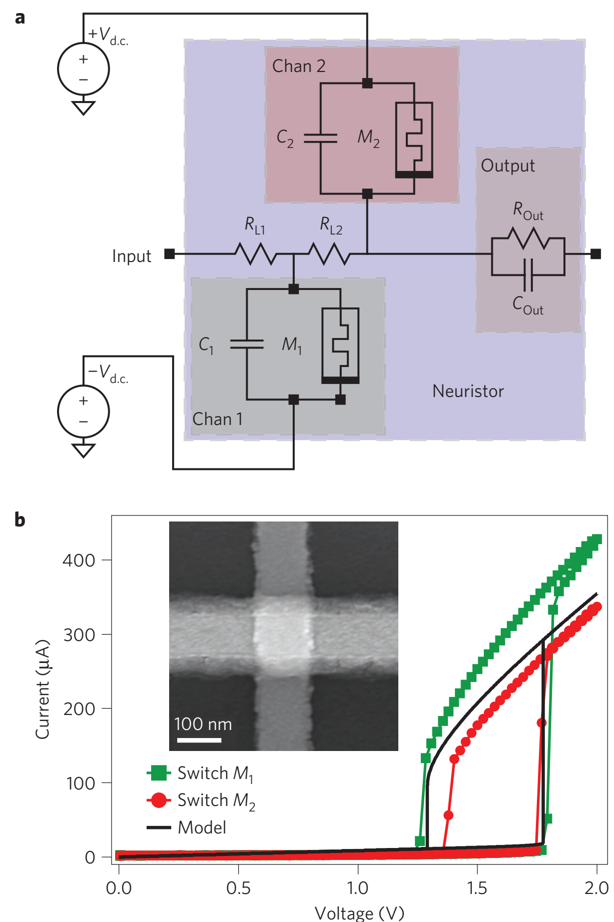

Figure 1 | Neuristor diagram and Mott memristor device characteristics. **a**, Circuit diagram of the lumped neuristor. The channels consist of Mott memristors (M_1 and M_2), each with a characteristic parallel capacitance (C_1 and C_2, respectively) and are biased with opposite polarity d.c. voltage sources. **b**, The bistable current–voltage curves of the two 110 × 110 nm^2 niobium dioxide crosspoint devices used in the experimental realization of the neuristor, with the inset showing a scanning electron micrograph of a typical device. The quasi-d.c. voltage-controlled current–voltage curve of the Mott memristor model used for simulations is also included in **b**.

mathematical framework for describing their behaviour[22]. Here we introduce the descriptive term Mott memristor for such devices because it specifies the physical process that governs their behaviour and differentiates them from other systems that exhibit threshold switching (that is, amorphous semiconductors[23]), which may not necessarily be memristors.

The functionally similar dynamical resistance behaviour of Mott memristors and Hodgkin–Huxley ion channels suggests that the

HP Labs, Palo Alto, California 94304, USA. *e-mail: Matthew.Pickett@hp.com.

© 2013 Macmillan Publishers Limited. All rights reserved

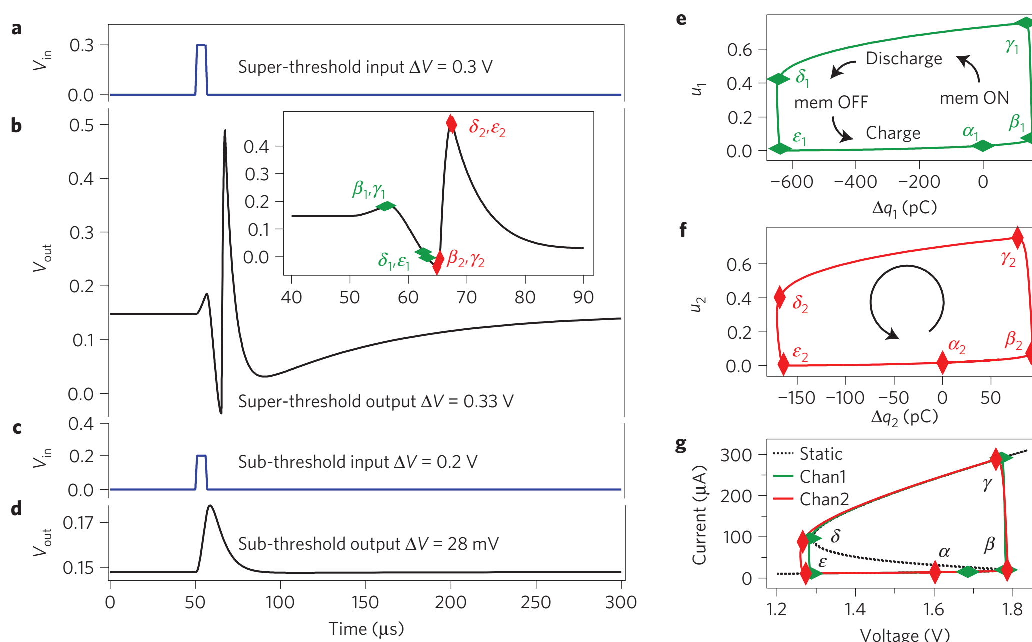

Figure 2 | All-or-nothing response and state variable dynamics of the neuristor. a,**b**, Simulated super-threshold 0.3 V input pulse (**a**) and its corresponding spike output (**b**). The magnified spiking region (**b**, inset) highlights the time sequence of events for channels one and two. **c**,**d**, A sub-threshold 0.2 V input (**c**) to the same device yields an attenuated output (**d**). **e**,**f**, Phase portraits of the characteristic state variables u and q for channel 1 (**e**) and channel 2 (**f**) illustrate a stable trajectory for both channels during the spike activation period of **b**. Points labelled α to ε on the phase portraits indicate the special points associated with switching events in each channel. **g**, Trajectories around the quasi-static current–voltage curve illustrate the conductive state of the respective Mott memristor for each channel at each point of interest. A descriptive time-series animation of the sequence of state variable and action potential events is available in the Supplementary Information.

former could serve as electronic analogues (rather than exact replicas) to emulate an axon action potential, particularly in the form of a neuristor[9]. A neuristor captures the features essential for action-potential-based computing: threshold-driven spiking, lossless spike propagation at a constant velocity with uniform spike shape and a refractory period. From a technological standpoint, neuristors based on Mott memristors are interesting because they switch rapidly ($\lesssim$1 ns) with low transition energy ($\lesssim$100 fJ), scale at least to tens of nanometres, are compatible with conventional front- or back-end complementary metal–oxide–semiconductor materials and processes, and can be fabricated on arbitrary substrates[22]. These properties stand in stark contrast to previously demonstrated neuristors based on voltage-controlled negative differential resistance devices (for example, Esaki diodes), because such designs required inductors to operate[11,13] and consequently cannot be integrated at the nanoscale.

The neuristor circuit introduced here (Fig. 1a) uses two nominally identical Mott memristors (M_1 and M_2), each of which has a parallel capacitor (C_1 and C_2, respectively). The two channels are energized (d.c.-biased) with opposite polarity voltages, similar to the sodium and potassium channels of the Hodgkin–Huxley model, and are coupled to each other through a load resistor (R_{L2}). The circuit has an input resistance (R_{L1}) and output impedance (R_{Out} and C_{Out}). This circuit is described by four coupled first-order differential equations that define four dynamical state variables (the same number as for Hodgkin–Huxley) for the system: the normalized metallic channel radii of the memristors u_1 and u_2 and the charges stored on the capacitors q_1 and q_2 (see Supplementary Information for mathematical details). The lumped neuristor can be considered as two coupled Pearson–Anson oscillators[24] energized below their oscillation threshold (d.c.-stable), which are activated by a sufficient perturbation on the input node (a.c.-unstable).

To explain the operating mechanism of the neuristor, we illustrate the all-or-nothing action potential response of the circuit by simulating two different input pulses. These inputs were voltage pulses that were coupled to the input node with a parallel RC impedance to simulate stimulus from an action potential generated by an upstream neuristor. We tracked the four state variables (u_1, q_1, u_2, q_2) as well as the currents and voltages at each node of the circuit to observe the sequence of events. Figure 2 presents the output voltage response of the neuristor excited by both super-threshold (0.3 V 10 μs) and sub-threshold (0.2 V 10 μs) voltage pulses. The super-threshold pulse excites an action potential with an amplitude of 0.33 V whereas the sub-threshold pulse is attenuated to 0.028 V, illustrating two important biomimetic properties: signal gain and thresholding.

Phase portraits (Fig. 2e,f) of the u and q state variables for both of the neuristor channels during spiking illustrate the sequence of physical events during the action potential. We plot the respective capacitor charges in terms of their deviation from their stable rest states $\Delta q = q - q_{rest}$. Both channels exhibit five points of interest (which we label as $\alpha - \varepsilon$) on their anticlockwise trajectories. At point α the channels are energized by the d.c. biases, but sit at their stable rest point $\Delta q = 0$. As the channel is excited away from rest, the channel capacitor charges (α to β) until the memristor threshold is triggered at point β. At this point and during the transition from β to γ the metallic channel radius increases rapidly and the Mott memristor resistance decreases accordingly, akin to the opening of an Hodgkin–Huxley ion channel. Afterwards, the capacitor discharges through the memristor from γ to δ. At point δ the memristor metallic channel radius decreases abruptly and the resistance jumps, emulating the closing of an ion channel. Once M_1 is fully insulating at point ε, the capacitor C_1 charges back to its rest state α. The relative speeds of each leg of the cycle are similar for both channels: the memristor switching is fastest ($\approx$1 ns) for both ON ($\beta - \gamma$) and OFF events ($\delta - \varepsilon$), the discharging process ($\gamma - \delta$) is moderate ($\approx$5 μs) and the charging process ($\varepsilon - \alpha$) is the slowest ($\approx$100 μs).

© 2013 Macmillan Publishers Limited. All rights reserved

NATURE MATERIALS DOI: 10.1038/NMAT3510

The sequence of events is offset in time for the channels, as is evident from the inset of Fig. 2b. The input pulse first triggers channel one by charging it from α_1 to β_1, after which it traverses to ε_1, which has the effect of depolarizing the output node. Subsequently, channel two is charged to point β_2, which initiates its trajectory to point ε_2 and results in the hyperpolarization of the output. A descriptive time-series animation of this process that tracks each state variable is available in the Supplementary Information.

Once the action potential has been initiated at β_1, the trajectories are relatively stable to perturbations and noise. This has the effect of enforcing a stable action potential period, because both channels must complete an orbit before another action potential can be generated, mimicking the refractory period of biological neurons. An alternative view of the switching cycle can be observed in Fig. 2g, which tracks the current through and voltage across the memristors during the action potential: during operation both devices traverse the bistable region of their current–voltage curves and switch sequentially to low resistance. The coupling between channel one and channel two (R_{L2}) must be conductive enough that the depolarization caused by the discharging of C_1 is sufficient to charge C_2 to point β_2. However, R_{L2} must also be resistive enough to ensure d.c. stability of the coupled system. If the input pulse is not large enough to push M_1 to its threshold voltage (β_1), the action potential does not fire and the state variables return to their resting states. Two other important biomimetic behaviours, constant spike amplitude/shape and constant velocity propagation through a series connection of neuristors, are demonstrated in simulation and included in the Supplementary Information.

An important property of biological neurons missing in many simplified models with a reduced number of system state variables is the diversity of spiking behaviours exhibited under the constant current-source configuration. We applied a 20 μA constant current bias to the input terminal and measured the spiking behaviours at the output for different combinations of channel capacitances, and compared the results to simulations. In Figure 3, we show three biomimetic spiking patterns:[25,26] regular spiking (Fig. 2b,c), chattering (Fig. 2d,e) and fast spiking (Fig. 2f,g). We see that our neuristor circuit can be easily modified to provide a variety of spiking behaviours, and that the simulations are in quantitative agreement with the experimental results.

Each spike train is characterized by different inter-spike intervals and spike widths (Δt) that are primarily controlled by the channel capacitances, C_1 and C_2 respectively, which were chosen to be large compared with the parasitic capacitance (≈100 pF) of the test apparatus. For an integrated circuit with much smaller parasitics, the capacitors could be scaled down to significantly decrease the spike energy ($1/2CV^2$) while increasing the frequency $(RC)^{-1}$. Ultimately, the operational speed of an integrated neuristor would be limited only by the switching speed of the Mott memristors, which can be less than 1 ns (ref. 22). A bifurcation diagram (Fig. 3h) for the output voltage of the fast-spiking neuristor was obtained by simulating the effect of sweeping the current-source magnitude. The bifurcation from monostable to spiking and back to monostable exhibits very abrupt thresholds, and the amplitudes of the spikes are nearly constant over the entire oscillation range. The inhibition threshold occurs when the d.c. bias is sufficient to force M_1 to remain open and has a biological equivalent[16]. We included four experimental data points on the bifurcation diagram taken from the fast-spiking neuristor, which demonstrates the sharp onset of spiking. The rectangular shape of the bifurcation region comes from the abrupt voltage threshold of the memristors, and provides uniformity for the device output independent of the input signal.

There are many interesting applications of neuristors for transistorless nanocircuits. They may be used as a signal repeater on a transmission line, in analogy with a node of Ranvier on an axon. Parallel neuristor circuits can be used as active transmission lines

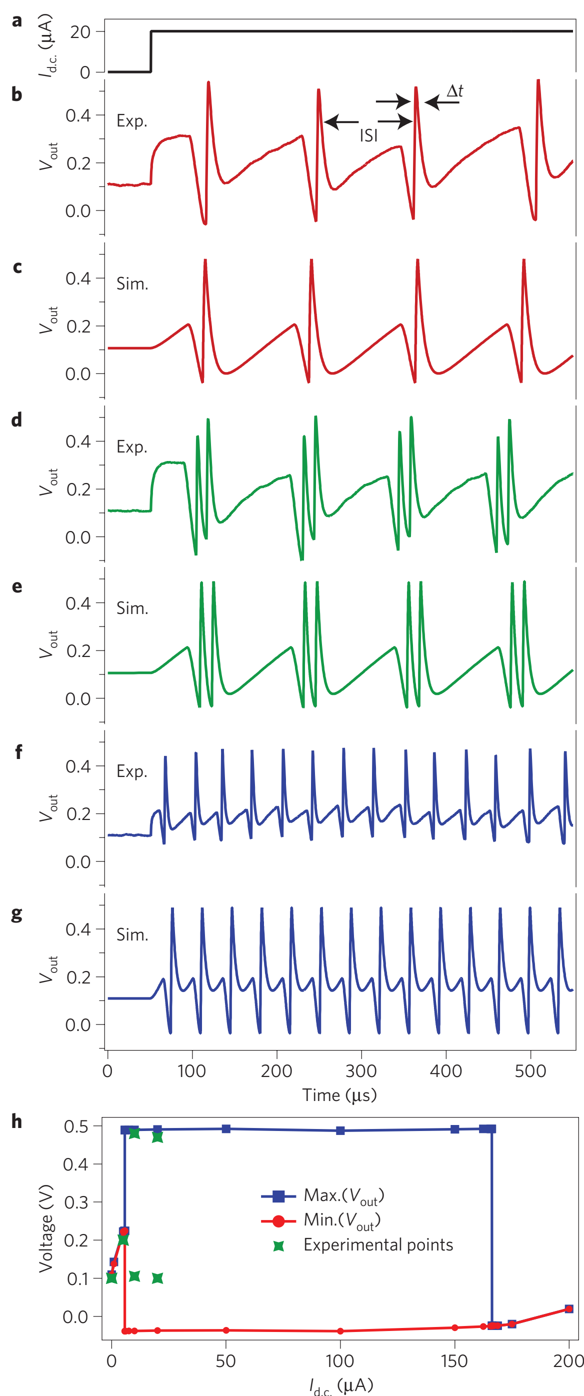

Figure 3 | Experimental and simulated spike trains. a–g, Experimental (**b**,**d**,**f**) and simulated (**c**,**e**,**g**) voltage outputs of a current-sourced neuristor with constant input $I_{d.c.} = 20$ μA (**a**). As the channel capacitances C_1 and C_2 are adjusted, the inter-spike interval (ISI) and spike width (Δt) are modified such that the neuristor exhibits: regular spiking ($C_1 = 5.1$ nF, $C_2 = 0.75$ nF) (**b**,**c**), chattering ($C_1 = 5.1$ nF, $C_2 = 0.5$ nF) (**d**,**e**) and fast spiking ($C_1 = 1.6$ nF, $C_2 = 0.5$ nF) (**f**,**g**) modes of operation. C_1 controls the inter-spike intervals and C_2 controls the spike width (Δt). **h**, The simulated bifurcation diagram for the fast-spiking circuit (**g**) presents the spiking amplitude as a function of current-source magnitude along with experimental points just above and below the initiation threshold. The spiking thresholds are sharp and no chaotic behaviour was observed near the thresholds. Unlike the Hodgkin–Huxley model, the output amplitude is flat for both minimum and maximum spike voltages over the entire range of the bifurcation current.

© 2013 Macmillan Publishers Limited. All rights reserved

and filters or as a basic building block for cellular neural networks[27]. Branched neuristors can be used for extremely large compact signal fan-out to thousands of terminals. By virtue of their biomimetic threshold spiking behaviour, neuristor circuits could be used to implement alternative computing schemes including neuristor logic[28], polychronous wavefront computation[29] and spike-based learning in non-volatile memristor networks[30–32]. We note that previous neuromorphic designs in which non-volatile memristors were used as synapses are orthogonal and complementary to the results presented here: those designs require active elements such as op amps to drive synaptic learning of the memristor synapses and make inferences from their state. The neuristors presented here have a transient memory but could replace the active elements in spike-based circuits[30–32], enabling a completely transistor-free neuromorphic architecture. Implementing such architectures will require low device variability in large integrated circuits and low leakage currents in the rest state. Leakage currents can in principle be low because the memristors are insulating in the neuristor rest state, and materials with a lower Mott transition temperature can be chosen to lower the switching threshold voltage[19] and thus reduce the power consumption.

We have demonstrated the biomimetic properties of a neuristor based on nanoscale Mott memristors, including all-or-nothing spiking of an action potential, a bifurcation threshold to a continuous spiking regime, signal gain and a refractory period. In this design, Mott memristors are electronic and inorganic analogues of ion channels found in biological neurons. These neuristors are compatible with existing integrated circuit processing and materials for hybrid circuits with transistors, but may be used to implement transistorless circuits and computational schemes. By constructing and testing biomimetic systems, neuristors may provide further insight into the signal and information transduction in the nervous system.

Methods

The memristors for the experimental demonstration of this circuit were crosspoint devices fabricated using nanoimprint lithography. A 110-nm-wide, 11-nm-thick bilayer (2 nm Ti/9 nm Pt) bottom electrode was patterned on a SiO_2 substrate with a liftoff process. This was followed by a blanket deposition of 30-nm-thick amorphous Nb_2O_5 grown by room-temperature reactive sputtering. Finally, a 110-nm-wide, 11-nm-thick Pt top electrode was patterned with a liftoff process perpendicular to the bottom electrode to yield the resulting $110 \times 110\,nm^2$ Pt/Nb_2O_5/Pt device stack (Fig. 1b). After fabrication, the devices were subjected to a +6 V, 1 μs electroforming pulse to create a locally reduced conduction channel of NbO_2, a Mott insulator[18]. The current–voltage plot in Fig. 1b shows the bistable current–voltage characteristics of the memristors used to construct the neuristor plotted together with the quasi-static curve obtained from the model used for simulation. See ref. 22 and Supplementary Information for numerical details of the model including the values used for the materials parameters. There were variations from device to device, as visible in Fig. 1b, but all simulations used a single model for the memristors and produced excellent agreement with the experimental data. The simulations were performed with the LTSPICE IV software package using the Mott memristor subcircuit defined in ref. 22. The experimental neuristor circuit was constructed by bread-boarding the two memristors with the requisite resistors and capacitors, as in Fig. 1a.

Received 30 May 2012; accepted 30 October 2012; published online 16 December 2012

References

1. Hodgkin, A. L. & Huxley, A. F. A quantitative description of membrane current and its application to conduction and excitation in nerve. *J. Physiol.* **117,** 500–544 (1952).
2. Herz, A. V. M., Gollisch, T., Machens, C. K. & Jaeger, D. Modeling single-neuron dynamics and computations: A balance of detail and abstraction. *Science* **314,** 80–85 (2006).
3. O'Reilly, R. C. Biologically based computational models of high-level cognition. *Science* **314,** 91–94 (2006).
4. Izhikevich, E. M. Hybrid spiking models. *Phil. Tran. R. Soc. A* **368,** 5061–5070 (2010).
5. Mead, C. *Analog VLSI and Neural Systems* (Addison-Wesley, 1989).
6. Rachmuth, G. & Poon, C. S. Transistor analogs of emergent iono-neuronal dynamics. *HFSP J.* **2,** 156–166 (2008).
7. Brüderle, D. *et al.* A comprehensive workflow for general-purpose neural modeling with highly configurable neuromorphic hardware systems. *Biol. Cybernet.* **104,** 263–296 (2011).
8. Arthur, J. V. & Boahen, K. A. Silicon-neuron design: A dynamical systems approach. *IEEE Trans. Circuits Syst. I* **58,** 1034–1043 (2011).
9. Crane, H. D. The neuristor. *IRE Trans. Elect. Comput.* **9,** 370–371 (1960).
10. Cote, A. J. A neuristor prototype. *Proc. IRE* **49,** 1430–1431 (1961).
11. Nagumo, J., Arimoto, S. & Yoshizawa, S. An active pulse transmission line simulating nerve axon. *Proc. IRE* **50,** 2061–2070 (1962).
12. FitzHugh, R. Impulses and physiological states in theoretical models of nerve membrane. *Biophys. J.* **1,** 445–466 (1961).
13. Nishizawa, J-I. & Hayasaka, A. Two-line neuristor with active element in series and in parallel†. *Int. J. Electr.* **26,** 437–469 (1969).
14. McCulloch, W. S. & Pitts, W. A logical calculus of the ideas immanent in nervous activity. *Bull. Math. Biophys.* **5,** 115–133 (1943).
15. Chua, L. & Kang, S. Memristive devices and systems. *Proc. IEEE* **64,** 209–223 (1976).
16. Chua, L., Sbitnev, V. & Kim, H. Hodgkin–Huxley axon is made of memristors. *Int. J. Bifur. Chaos* **22,** 1–48 (2012).
17. Chua, L. O. Local activity is the origin of complexity. *Int. J. Bifur. Chaos Appl. Sci. Eng.* **15,** 3435–3456 (2005).
18. Chudnovskii, F. A., Odynets, L. L., Pergament, A. L. & Stefanovich, G. B. Electroforming and switching in oxides of transition metals: The role of metal–insulator transition in the switching mechanism. *J. Solid State Chem.* **122,** 95–99 (1996).
19. Chopra, K. L. Current-controlled negative resistance in thin niobium oxide films. *Proc. IEEE* **51,** 941–942 (1963).
20. Geppert, D. V. A new negative-resistance device. *Proc. IEEE* **51,** 223–223 (1963).
21. Pickett, M. D., Borghetti, J., Yang, J. J., Medeiros-Ribeiro, G. & Williams, R. S. Coexistence of memristance and negative differential resistance in a nanoscale metal-oxide-metal system. *Adv. Mater.* **23,** 1730–1733 (2011).
22. Pickett, M. D. & Williams, R. S. Sub-100 femtoJoule and sub-nanosecond thermally-driven threshold switching in niobium oxide crosspoint nanodevices. *Nanotechnology* **23,** 215202 (2012).
23. Ielmini, D. Threshold switching mechanism by high-field energy gain in the hopping transport of chalcogenide glasses. *Phys. Rev. B* **78,** 035308 (2008).
24. Pearson, S. O. & Anson, H. S. G. Demonstration of some electrical properties of neon-filled lamps. *Proc. Phys. Soc. Lond.* **34,** 175 (1921).
25. Connors, B. W. & Gutnick, M. J. Intrinsic firing patterns of diverse neocortical neurons. *Trends Neurosci.* **13,** 99–104 (1990).
26. Izhikevich, E. M. Simple model of spiking neurons. *IEEE Trans. Neural Net.* **14,** 1569–1572 (2003).
27. Chua, L. O. & Yang, L. Cellular neural networks: Applications. *IEEE Trans. Circuits Syst.* **35,** 1273–1290 (1988).
28. Wilamowski, B. M. A novel concept of neuristor logic. *Int. J. Electron.* **33,** 659–663 (1972).
29. Izhikevich, E. M. & Hoppensteadt, F. C. Polychronous wavefront computations. *Int. J. Bifur. Chaos* **19,** 1733–1739 (2009).
30. Snider, G. S. Self-organized computation with unreliable, memristive nanodevices. *Nanotechnology* **18,** 365202 (2007).
31. Choi, H. *et al.* An electrically modifiable synapse array of resistive switching memory. *Nanotechnology* **20,** 345201 (2009).
32. Pershin, Y. V. & Ventra, M. D. Experimental demonstration of associative memory with memristive neural networks. *Neural Netw.* **23,** 881–886 (2010).

Acknowledgements

We acknowledge J. Borghetti for seeding important discussions on biological oscillators with the authors; X. Li, C. Le and T. Ha for fabrication and laboratory support; and J. P. Strachan for review and discussion of the manuscript.

Author contributions

M.D.P. conceived, simulated, fabricated and tested the neuristor described in this work. R.S.W. guided the work and provided critical insight. G.M-R. provided discussion and analysis of results and essential management support. M.D.P. and R.S.W. wrote the manuscript.

Additional information

Supplementary information is available in the online version of the paper. Reprints and permissions information is available online at www.nature.com/reprints. Correspondence and requests for materials should be addressed to M.D.P.

Competing financial interests

The authors declare no competing financial interests.

© 2013 Macmillan Publishers Limited. All rights reserved